Visual Beat (Moiré) Effects in Nature and in Optical Metrology

Ariana Ray, Hastings-on-Hudson, October 2012

1 Introduction

When two tuning forks of slightly different pitch are struck at the same time, a distinct, undulating sound can be heard quite clearly, created by the separate notes of the tuning forks. This phenomenon is an example of the "beat effect." The beat effect occurs when two regular patterns, such as sound waves, of slightly different periods overlap: at times, the maxima of the patterns will coincide, creating increased maxima, and at times the minima will coincide, forming exaggerated minima. The overall result is that a new, magnified regular pattern emerges from the slight displacement of the two original patterns.

The beat effect is not simply limited to a dissonance between tuning forks, however. Examples of applications of the beat effect include the Vernier, a device that can measure extremely small increments to a great deal of accuracy [1], the police RADAR gun, which is a quick method of vehicle speed measurement [2], and the Doppler Pulse Probe, a method of detecting the weak pulse of a premature infant [3].

There are also a variety of beat effects that manifest themselves as striking visual patterns. These effects are called "moiré effects," and they are a mathematically intriguing optical phenomenon with a wide range of applications. Moiré patterns are frequently observed when two objects with partially-transparent repetitive designs, such as window screens or chain-link fences, overlap. When one pattern is tilted with respect to the other or has a different period, lines overlap to create exaggerated light and dark areas. As a result, intricate patterns appear to coalesce on the surface. The word "moiré" is speculated to have originated from the Latin word"marmoreus," "marbled," before morphing into the English "mohair," and finally the French verb "moirer," meaning "to produce a watered textile by weaving or pressing" [4]. The resulting English noun "moiré" refers to the fabric produced by such a process. Moiré fabrics, such as watered silk, have been revered since the Middle Ages for the rippled "watermarks" created by their unique weave [5].

Many famous paintings, such as "Peter I of Russia," showcase examples of the moiré-like effect in cloth. Applications of moiré effects include interferometry [6], strain measurement and topography [7], collimation testing [8], and focal length measurement [9]. Even more surprising uses can be found in navigation [10], steganography [11], and counterfeit prevention [12]. More recently, moiré patterns have aided researchers in studying the structure of graphene, a material with rather exceptional properties, that was the subject of the 2010 Nobel Prize in Physics [13]. Moiré patterns seen in graphene magnify the structure of the carbon lattice and can be used to detect minute amounts of strain in graphene and other materials [14].[1]

In this work, the moiré effect has been studied both theoretically, through mathematical simulations, and experimentally, through an optical application. In the first part of this work, various types of moiré patterns were modeled using *Mathematica*, which is a mathematical computing software commonly used in scientific work for generating graphics and doing calculations [16]. The resulting animations are both informative about and instructive on the subject of moiré patterns. The second part of this work focused on one of the applications of the moiré effect: collimation testing. Beam collimation is one of the more important applications of the moiré effect, as collimation is often essential in an optical experiment. Pursuant to the two different aspects of this work, this paper is divided into two sections: the first describes the models of the moiré effect that were created (§2), and the second discusses the collimation tester and the theory behind it (§3).

2 Modeling the Moiré Effect

2.1 Methods

We first explored a variety of moiré effects and ways to create them. In particular, we have experimented with gratings that are not linear or that are not strictly periodic (quasiperiodic). The experiments consisted of creating virtual gratings of different pitch and overlapping them using

[1] Moiré-like effects can also have undesirable consequences, such as the creation of artifacts ("aliasing") in digital images or sound recordings. Aliasing occurs so frequently in digital photographs that manufacturers of digital cameras have introduced "anti-aliasing filters" into their cameras to attenuate the effect of aliasing [15].

Mathematica to study the resulting patterns. Four different periodic gratings were employed: lines, concentric ellipses, concentric circles, and arrays of dots. A quasiperiodic grating was also studied. It consisted of an array of dots arranged like florets on a sunflower and was generated using Vogel's formula (2004) [17]. All models were animated using the *manipulate* tool in *Mathematica* to allow for user interaction.

2.2 Linear Gratings

Linear moiré is moiré created with linear gratings. This form of moiré was modeled first, as it is the most studied of all forms of moiré patterns. Linear moiré is an excellent visual example of the beat effect, as it can be created by overlapping two linear gratings of different periods. It can be shown [18] that if the first grating has a period λ_1 and the second, a period of λ_2, then the period of the resulting moiré fringes is

$$\lambda_{beat} = \frac{\lambda_1 \lambda_2}{\lambda_2 - \lambda_1} \qquad [1]$$

This equation can be derived from the formula used to determine the beat frequency of two interfering sound waves, $f_{beat} = |f_1 - f_2|$. Indeed, if one imagines that the linear gratings are instead sine or cosine functions, with the dark lines as maxima and the light spaces as minima, it is simple to see how fundamentally linear moiré and beat frequencies created by two sound waves are related.

It can be shown [18] that the shape of the moiré fringes created by two gratings with period λ_1 and λ_2 follows the form

$$\cos(\phi_1(x, y) - \phi_2(x, y)) \qquad [2]$$

where $\phi_1(x, y)$ and $\phi_2(x, y)$ represent the grating functions of the two linear gratings. Then, if the two gratings are overlaid with an angle of 2α between them, the grating functions $\phi_1(x, y)$ and $\phi_2(x, y)$ can be written as

$$\phi_1(x, y) = \frac{2\pi}{\lambda_1}(x \cos\alpha + y \sin\alpha) \qquad [3]$$

$$\phi_2(x, y) = \frac{2\pi}{\lambda_1}(x \cos\alpha - y \sin\alpha) \qquad [4]$$

From here, one can simplify Eqn. [2] by rewriting the argument in the *cosine* function as:

$$\phi_1(x,y) - \phi_2(x,y) = \frac{2\pi}{\lambda_{beat}} x\cos\alpha + \frac{4\pi}{\overline{\lambda}} y\sin\alpha \qquad [5]$$

where $\overline{\lambda}$ is the average line spacing [18]. Now, the locations of the centers of the moiré fringes are given by

$$\phi_1(x,y) - \phi_2(x,y) = M2\pi \qquad [6]$$

where M is the fringe order (the integer corresponding to a fringe; ie, for the first fringe, $M = 1$). Creath and Wyant [18] described two special cases for Eqn. [5]: when $\lambda_1 = \lambda_2 = \lambda$, and when $\alpha = 0$. The former case was studied first.

When the periods of the two gratings are the same, λ_{beat} in Eqn. [1] is seen to become infinite, and thus the first term of Eqn. [2] will go to zero. Therefore, the x-component of Eqn. [2] is eliminated, and the shape of the resulting moiré fringes is dependent only on the y-component:

$$\phi_1(x,y) - \phi_2(x,y) = \frac{4\pi}{\overline{\lambda}} y\sin\alpha \qquad [7]$$

One can also solve for this mathematically: when the periods of the gratings are the same, it follows that $\overline{\lambda}$ is equal to λ. By setting Eqn. [7] equal to Eqn. [6] (solving for the locations of the fringe centers), one obtains the following equation:

$$M\lambda = 2y\sin\alpha \qquad [8]$$

The case of $\lambda_1 = \lambda_2 = \lambda$ was modeled using *Mathematica*. Two sets of parallel lines were plotted to represent the gratings. These sets of lines had different slopes to mimic the rotation of one grating with respect to the other. α can be found in terms of the slopes of the two lines

$$\tan(2\alpha) = \frac{m_1 - m_2}{1 + m_1 m_2} \qquad [9]$$

where m_1 and m_2 are the respective slopes of the two sets of parallel lines.

If the sets of parallel lines that comprise the two gratings are taken to follow the equations $y_1 = m_1 x - ct$ and $y_2 = m_2 x - ct$ respectively, where t is the iterating value, then one can solve for the periods of the gratings. This is done by setting y equal to zero and solving for x. It becomes apparent that, left as is, the two gratings will have different periods, as $\lambda_1 = \frac{ct}{m_1}$ and $\lambda_2 = \frac{ct}{m_2}$. This can be corrected by multiplying the c value of y_1 by $\frac{m_1}{m_2}$. The model was animated with the *manipulate* function to allow the user to control the slopes of the two gratings, the scale of the plot, and the horizontal displacement of one grating with respect to the other. Figure 1 (a) shows a screenshot of the output of the *Mathematica* code. The model displayed the expected horizontal fringes when one grating was tilted with respect to the other. In addition, there appeared to be horizontal fringes when λ_1 was an integer multiple of λ_2 (i.e. $\lambda_1 = a\lambda_2$). This was surprising, as Eqn. [1] would not go to infinity in this case and cause the first term of Eqn. [5] to vanish. A screenshot of the case of $\lambda_1 = 2\lambda_2$ is shown in Fig. 1 (b).

The second special case, when $\alpha = 0$, was also looked at briefly. Two gratings with a very slight difference in period were plotted by vertical lines on *Mathematica*. Users move one grating horizontally in the negative or positive direction to see the resulting fringe shift. In the case where the gratings are not tilted with respect to each other, the second term of Eqn. [2] and the *cosine* of

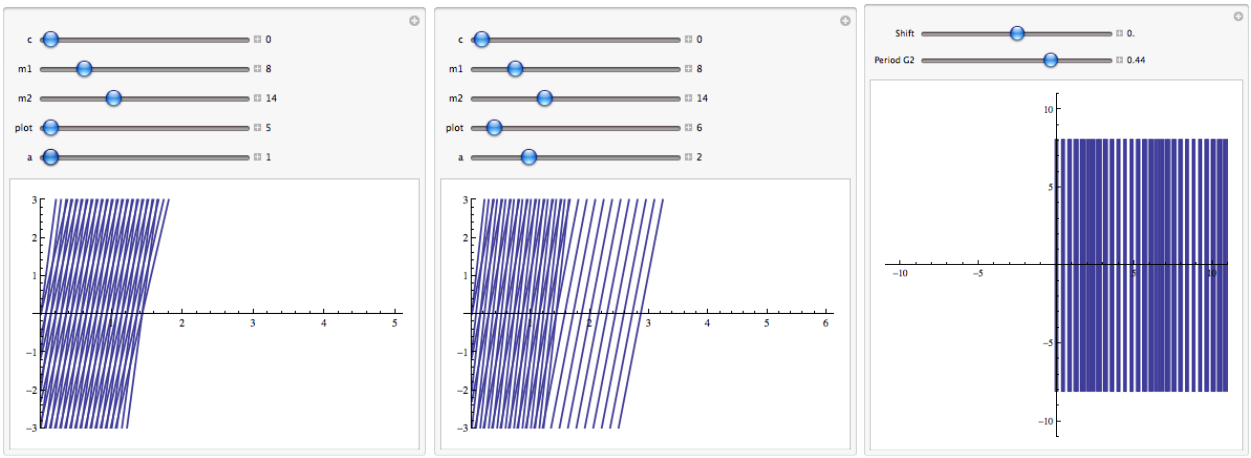

Figure 1: (a) Left: *Mathematica* output showing a simulated moiŕe pattern for $\lambda_1 = \lambda_2$. (b) Center: The same, but for $\lambda_1 = 2\lambda_2$. The top panels in each figure allow the user to control, in order, the relative horizontal displacements of the two gratings (c), line slopes (m_1, m_2), the scales of the plots, and the integer ratio a of λ_1 to λ_2. The case of $a = 2$ is shown in (b). Notice the horizontal fringes in each image. The axes scales are in arbitrary units. (c) Right: *Mathematica* output showing a simulated moiŕe pattern for the case of $\alpha = 0$. The axes units are arbitrary. The period of the second grating (G2) is changed by the user. Note the vertical fringes, as expected from Eqn. [11]

the first term vanish. The grating equation becomes:

$$\phi_1(x,y) - \phi_2(x,y) = \frac{2\pi}{\lambda_{beat}}x \qquad [10]$$

By setting Eqn. [10] equal to Eqn. [6], one obtains the equation:

$$M\lambda_{beat} = x \qquad [11]$$

Because there is no y-component to this equation, the resulting moiré fringes should not change as y changes. This implies that the fringes observed are vertical, as seen in Fig. 1 (c).

2.3 Nonlinear Gratings

While linear moiré is fascinating, one must look at nonlinear gratings to see truly surreal moiré patterns. Two forms of nonlinear gratings were studied: gratings comprised of lines (circular, elliptical) and gratings comprised of arrays of dots.

Among the first to study moiré patterns created with nonlinear gratings was Oster et al. (1963) [19], in a paper that described the mathematics behind moiré patterns created with combinations of various linear and nonlinear gratings.

One of the cases that was studied by Oster et al. was that of two gratings of equispaced concentric circles. It was shown that when two gratings comprised of concentric circles are superimposed and shifted with respect to each other, the resulting fringes take the shape of hyperbolas with a focus at the center of each circle. When the gratings are further distanced, an ellipse forms between the hyperbolas. Motivated by these results, gratings comprising concentric circles were created using *Mathematica*. As with the linear models, this model was animated, allowing users to change the number of concentric circles in each grating (thus changing the period of the grating) and the horizontal and vertical displacement of the gratings with respect to each other, as illustrated in the screenshot shown in Fig. 2 (a). It was seen that, indeed, the moiré patterns formed were in the shape of hyperbolas, and an ellipse was formed in the center when the gratings were moved

sufficiently far apart.

From circular gratings, it seemed logical to create elliptical gratings and similarly animate the models. Two types of concentric elliptical gratings were created. In the first, the semi-major and semi-minor axes were varied in a ratio that could be changed by the user, so that the resulting ellipses were truly concentric. In the second, the semi-major axis was kept the same, but the semi-minor axis was varied, creating a grating that looked like a cat's eye. Figures 2 (b) and 2 (c) show the screenshots of the *Mathematica* output for these cases. Although the two types of gratings themselves appeared to be rather similar, the moiré patterns created had a very discernible dissimilarity between them.

Another genre of grating simulated was the dot array. This was motivated by the discovery in the lab of several thin squares of metals with holes punched out in a regular rectangular pattern. When one such square was placed on top of another square and tilted, moiré patterns that looked like a magnified form of the holes punched out in the squares appeared as if from nowhere.

A similar dot array was modeled using *Mathematica*. Two such gratings were created and overlapped using the *Prolog* function [16], and animated so that the user determined the number of dots in each grating. Horizontal and vertical shifts were added to center one grating with respect

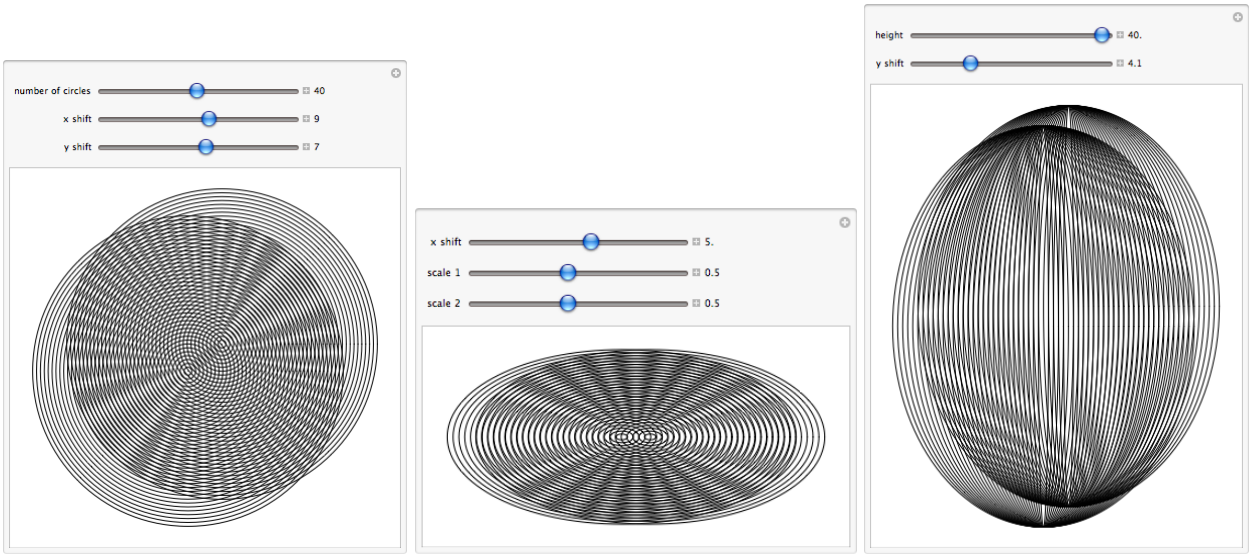

Figure 2: (a) Left: *Mathematica* output showing a simulated moiŕe pattern for gratings comprising concentric circles. (b) Center: The same, but for concentric ellipses. (c) Right: Moiré pattern for elliptical gratings where the semi-major axes are kept constant. Notice the markedly different patterns seen in (b) and (c). In each figure the panels at the top allow the user to control the scale factors of the ellipses and the displacements of the gratings.

to the other.

These gratings were modified so that the user could change the horizontal or vertical scale of one grating with respect to the other. The resulting fringes were similarly elongated or compressed. Figure 3 (a) shows a screenshot of the *Mathematica* output for gratings comprising dot arrays with a width to length ratio of 1. In Fig. 3 (b), the user has the option to vary the width to length ratio of the second grating. Moiré patterns created when one dot array is tilted with respect to the other are shown in Fig. 3 (c). The pattern observed is similar to that seen for the mesh gratings found in the lab, as shown in Fig. 3 (d).

The dots in Fig. 3 have rectangular packing, which affects the resulting moiré patterns. There are, however, other methods of packing dots in an array. One particularly space-efficient form of packing is hexagonal packing, which is frequently seen in nature, such as in crystalline structures. For example, iron in FeO and Pt (111) are both packed hexagonally, which is more space-efficient than rectangular packing. When very thin layers of FeO and Pt(111) are overlapped, triangular-shapes moiré patterns can be observed [20].

A similar scenario was modeled by generating two dot arrays packed in a hexagonal manner. This is illustrated in Fig. 4 (a). Each of the dot arrays were formed by adding together two other identical arrays to form the final hexagonal grid, which was created as follows: First, a grid of 1×2 rectangles (y is twice x at any given dot) was modeled. Then, a replica of this grid was superimposed on the first and shifted along the x-axis and the y-axis by half the length of the respective sides. The moiré patterns were generated by compressing one grid equally in both axes. As expected, triangular moiré was observed. This can be compared to the triangular moiré created by the overlap of FeO and Pt(111) (Fig. 4(b)). The dot arrays were similar to linear gratings in that a greater difference in period (a greater compression) created more moiré patterns in a given area.

2.4 Quasiperiodic Gratings

All the gratings previously studied were periodic in some shape or form, but moiré patterns do not necessarily have to be formed by periodic gratings. Aperiodic (random) gratings can also create

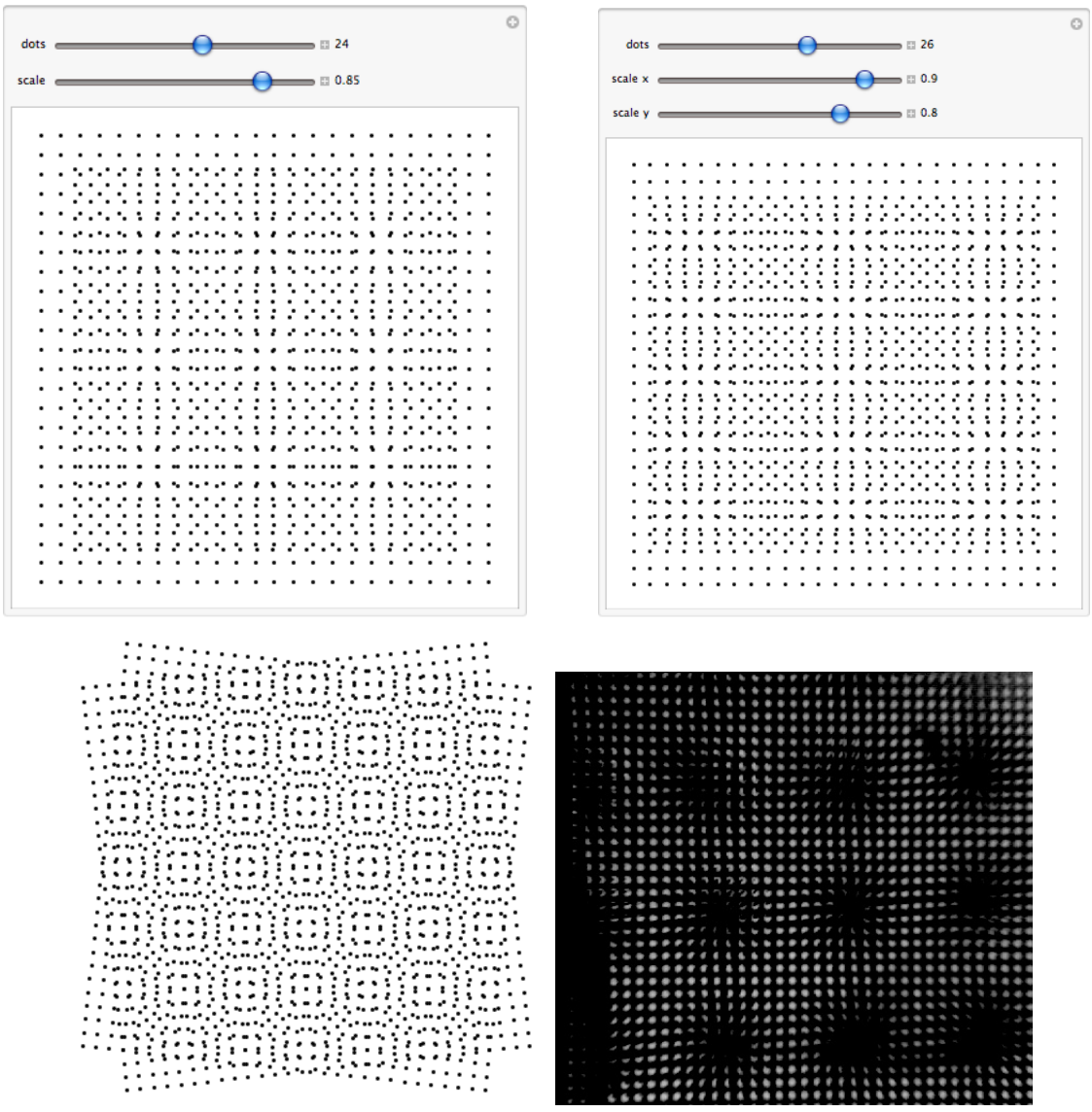

Figure 3: *Mathematica* output showing a simulated moiŕe pattern for several different dot arrays. (a) Top left: gratings with width to length ratio of 1. (b) Top right: width to length ratio of the second grating variable. The figure shows the particular case of 9:7. (c) Bottom left: Tilted gratings. (d) Bottom right: Grating found in the lab. The grating is shown to scale. Note the similarity between the moiré patterns observed here and those observed in the bottom left image (c).

moiré patterns, called "Glass patterns" [21]. One can achieve aperiodicity by creating an array of randomly placed dots; Glass and Pérez [21] created aperiodic gratings by splattering paint on a transparency. If the random dot pattern is placed on top of its copy and tilted, moiré patterns can be observed.

It was more recently observed that Glass patterns can be made to have any shape [22]. If the dots in one random array are replaced with any shape, for example, the number "2," and then

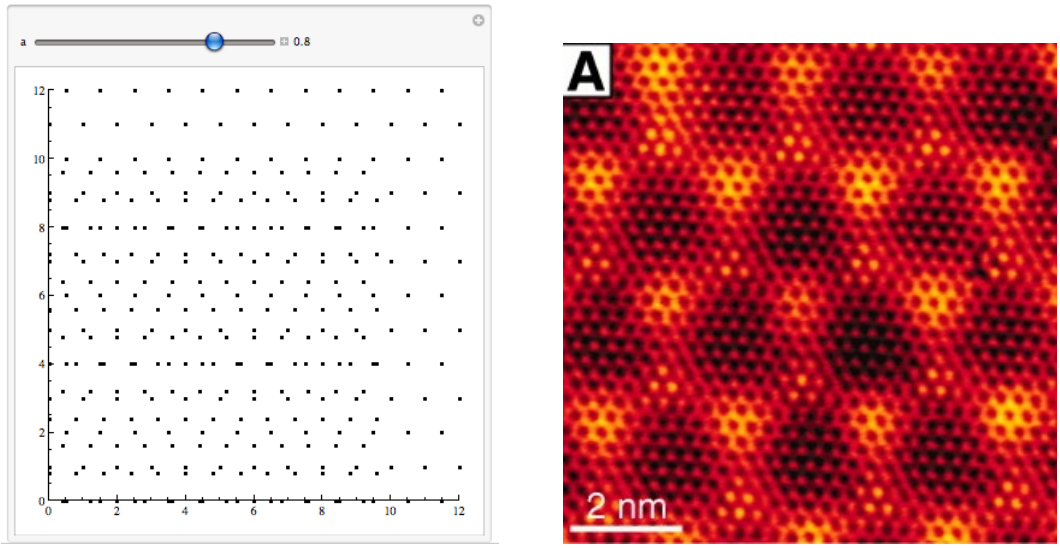

Figure 4: (a) Left: *Mathematica* output showing a simulated moiŕe pattern for a hexagonal grid demonstrated for a grid ratio of 10:8 for the two gratings. (b) Right: Moiré patterns formed by the overlap of thin layers of FeO and Pt(111). Figure taken from Merte et al. (2012) [20]. Note the similarities in the two patterns.

placed under an identical, but slightly tilted array that has holes punched out instead of printed dots, the moiré patterns take on the shape of a single, enlarged "2". This phenomenon extends to periodic arrays as well; however, in the case of periodically arranged dots, many smaller forms of "2" that repeat at regular intervals are seen, rather than a single large shape.

This fascinating effect prompted a question: if aperiodically arranged dots generate a single large form of the shape, and periodically arranged dots generate many smaller forms of the shape, what effect do quasiperiodically arranged dots have on Glass patterns?

The class of quasiperiodic patterns falls directly in between the class of random patterns and the class of periodic patterns. A quasiperiodic pattern is one that retains some structure, but lacks periodicity. This means that it does not have "translational symmetry"– if one were to put one quasiperiodic structure on top of another identical to it and move the top structure from left to right, there would be no other place at which the structures would be in perfect alignment. In contrast, consider a perfectly periodic structure, such as a picket fence or a sine wave. The structures would be in alignment after every period.

Quasiperiodic structures were very recently brought to widespread notice when the 2011 Nobel Prize in Chemistry was awarded for the discovery of "quasicrystals" [23]. Quasicrystals, crystals

that have quasiperiodic structures, were first observed in Aluminium-Manganese alloys in 1982, when the anomalous electron diffraction patterns produced by the alloys were noticed [24]. Many other compounds that have quasicrystalline structure have since been found. Indeed, the discovery of quasicrystals was so fundamental that the formal definition of a "crystal" had to be re-worded to include the concept of periodicity that had previously always been taken for granted.

Aside from quasicrystals, there is another famous example of a quasiperiodic structure– the Fibonacci sequence. This is generated by the rule: $F_n = F_{n-1} + F_{n-2}$ for $n \geq 3$, $F_1 = 1$, $F_2 = 1$ The Fibonacci sequence appears remarkably often in nature. The fruitlets of a pineapple, the scales of a pine cone, and the florets of a sunflower are all examples of natural objects that follow the Fibonacci sequence [25].

We decided that before looking at quasiperiodically generated Glass patterns, a quasiperiodic grating would be modeled. This quasiperiodic grating would be used to create moiré patterns in the same way that periodic gratings were previously used. After deliberation on how to create a quasiperiodic grating, it was decided that the grating should in some way be connected to the Fibonacci sequence, as the Fibonacci sequence itself is quasiperiodic. This connection was found by simulating the arrangement of florets on a sunflower. The formula for the layout of florets on a sunflower has been found to rely on the golden angle, which in turn relies on the Fibonacci

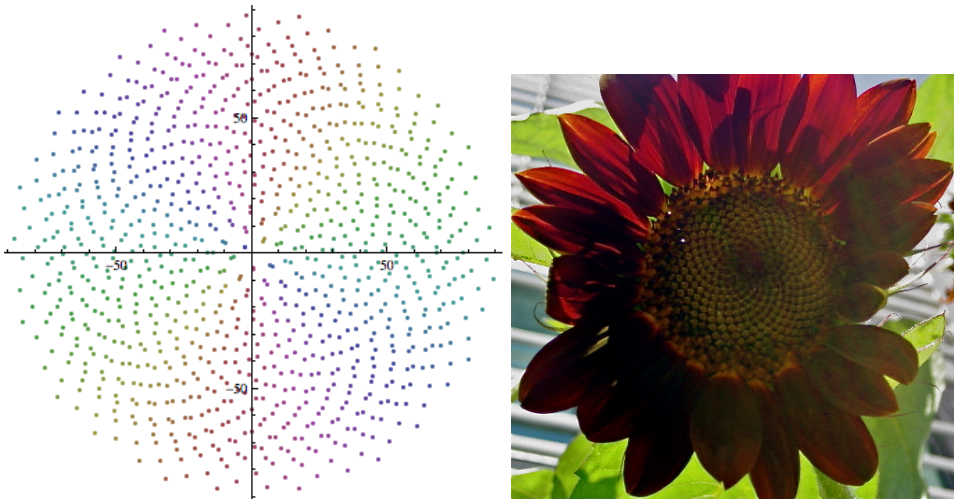

Figure 5: (a) Left: *Mathematica* output showing a simulated moife pattern for overlapping sunflower floret patterns which is an example of a quasiperiodic grating. The ratio of the two gratings in this example is 8:7. (b) Right: A photograph of a sunflower taken by the author (July 2012).

sequence, and was worked out by Vogel (1979) [17]. This makes the arrangement of florets on a sunflower quasiperiodic.

Vogel's formula, in polar coordinates, can be written as $\theta = \frac{2\pi}{\phi^2}n$, where $r = c\sqrt{n}$, c is the scale factor, ϕ is the golden ratio, and n is the counter. This equation was used to create a quasiperiodic grating to mimic a sunflower floret pattern. Figure 5 (a) shows the moiré pattern generated by overlapping two modeled sunflower florets. The index n takes the range [1, 500] and the ratio of the two gratings is 8:7.

3 Collimation Testing

The second major component of this research was testing the collimation of a laser beam. This is an excellent example of the applications of two fascinating optical phenomena: the moiré effect, and the Talbot effect (described below).

3.1 Collimation

Collimation in optics refers to obtaining parallel rays from a divergent beam of light emitted by a source. This can be achieved by placing a converging lens at its focal distance from the source; however, a beam will only be perfectly parallel forever if the source of light is a point source. In real life, it is not possible to have a point source, and thus the beam will eventually diverge. In this case, the definition of "collimation" becomes more nuanced. For the purposes of this discussion, however, a beam is collimated when the source is placed at the focal point of a lens, and when the waves leaving the lens are flat, i.e., have planar wavefronts. A high quality of laser beam collimation is often a necessity in optics research setups where great precision is required, but this is difficult to achieve. For example, a high degree of collimation is required in applications such as the Fourier transform generator, the optical coherent processor, and the image transformer [26].

A simple method of determining whether a beam is collimated involves placing a piece of paper in the path of the beam at various places and adjusting the setup so that the spot size does not differ

as the beam travels. This technique, however, is highly subjective, and an easier and more exact method would be preferable. Over the past few decades, significant research has been conducted to create optical setups that can test with high precision the collimation of laser beams. One intriguing idea involves a combination of the moiré and Talbot effects, two extremely interesting optical phenomena.

In this work, the Talbot and moiré effects have been used in a setup to test the collimation of a laser beam. While similar setups have been devised in the literature (see §3.3), the goal of this research is to model the setup and to quantify the parameters to obtain a systematic scheme for determining beam collimation.

3.2 Talbot Effect

The Talbot effect was first observed in 1836 by Henry Fox Talbot, one of the pioneers of photography [27]. Although Talbot himself did not pursue his observations very far, Lord Rayleigh continued the study of the Talbot effect in 1881. The Talbot effect occurs when a light beam is shone through a grating; a self image of the grating is formed at fixed distances (the Talbot distance) from the original grating, so long as the grating is still in the near field. In the far field, the self image is replaced with the expected textbook diffraction pattern.

Lord Rayleigh (1881) [28] showed that the Talbot distance could be written as

$$Z_T = \frac{2d^2}{\lambda} \qquad [12]$$

where d is the period of the grating and λ is the wavelength of the incident light. It was later found by Cowley and Moodie (1957) [29] and Winthrop and Worthington (1965) [30] that there exist fractional Talbot images as well. For example, at half the Talbot distance, an image of the grating forms shifted by half the grating's period. At a quarter of the Talbot distance, an image of the grating with half the period of the original grating forms; at an eighth, the period of the image is a fourth of the original, and so on. The set of all fractional images within one Talbot distance is called the "Talbot carpet." Considering the inherent self-similarity in the Talbot effect, it is not a

surprise that the Talbot carpet was later found to follow a fractal structure [31]. Talbot carpets have more recently been simulated on computers, resulting in colorful, vibrant fractal patterns.

3.3 Experimental Setup

The collimation test instrument is based in large part on previous collimation tester setups, such as those of Ganesan and Venkateswarlu (1993) [32], Kothiyal and Sirohi (1987) [8] and Silva (1980) [33]. A laser beam is collimated using a telescope and a Ronchi grating, and the collimation is analyzed using the moire effect, which has been described theoretically above (§2). A Ronchi grating is a specific type of grating in which the period is equal to twice the width of the slits. This method allows us to collimate a beam quickly and efficiently.

Figure 6 is a schematic diagram of the experimental setup. A 150 micron pinhole is placed 8.0 centimeters away from a 633 nm HeNe laser light source. Two lenses are arranged 15.0 centimeters from the pinhole, so that they act as a telescope. This telescope collimates the beam. The pinhole serves the purpose of reducing the noise in the resulting image by creating an Airy pattern the central part of which is similar to an ideal Gaussian beam. The first lens has a focal length of 25.4 mm, and the second, the collimating lens, has a focal length of 330 mm. In order for the laser beam to be collimated, the collimating lens must be placed so that its focus coincides with the focus of the first lens. If the collimating lens is moved closer to the first lens, then the beam will diverge, and vice versa. A Ronchi grating (50 lines/ inch) tilted about 3 degrees is placed 99.0 cm from the collimating lens. A retroreflector is placed at half of the grating's Talbot distance away from the grating. We have simplified the collimation test instrument by eliminating the beam splitter that was previously necessary. This increases the intensity of the resulting moiré effect.

Incident light passes through the grating and forms a self image as it hits the retroreflector, half the Talbot distance away. The self image is reflected twice, so that the returning light forms a self image of the grating reflected about the vertical. This oppositely tilted self image passes once more through the original grating, creating moiré fringes. A mirror placed just before the grating is angled so that it does not block any light, but reflects the fringes off to the side, where they

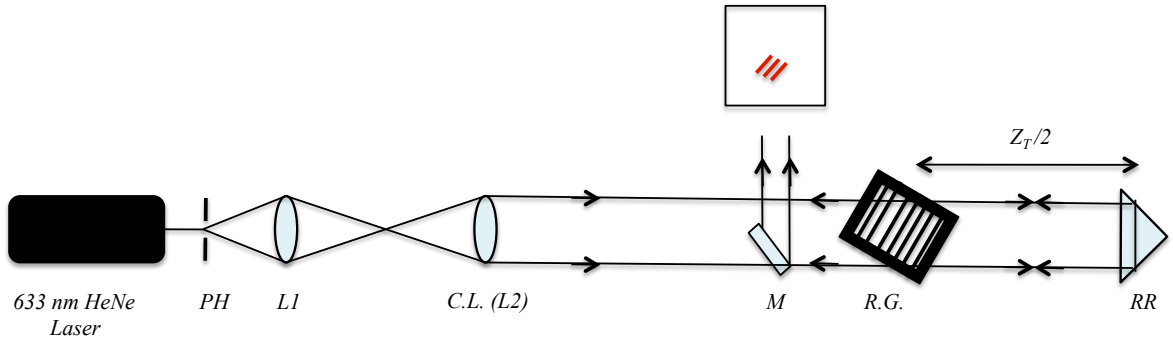

Figure 6: Schematic diagram showing the experimental setup to test beam collimation. The individual parts are labeled, as follows. PH: pinhole, L1: first telescopic lens, L2: Collimating lens (C.L.), M: mirror, R.G.: Ronchi grating, RR: retroreflector. The distance of the retro-reflector from the Ronchi grating is half the grating's Talbot distance. Z_T is the Talbot distance. The moiré are produced on the screen, as shown.

are photographed through white paper with a camera. The distance of the collimating lens from the first lens was varied from 41.5 cm to 45.4 cm in 1.0 mm steps, and the resulting moiré fringe patterns were recorded. Figure 7 shows a sample of 8 out of 40 images that were recorded.

As collimation decreases, the radius of curvature of the wavefront also decreases and the wavefront becomes spherical, creating either a divergent or a convergent beam. If the wavefront is spherical rather than planar, it follows that the resulting Talbot self image will be either magnified or diminished in size. This magnification of the image of the grating, or lack thereof, is equivalent to placing two gratings of different period on top of each other. Furthermore, the self image is tilted with respect to the original grating, so that the resulting moiré fringes will similarly tilt as the period of the self image changes. Following a formula given by Creath and Wyant (1992) [18], the tilt of the moiré fringes can be used to determine the difference in period between the grating and the self image:

$$\tan\theta = \frac{\lambda_1 + \lambda_2}{\lambda_2 - \lambda_1}\tan\alpha \qquad [13]$$

where θ is the angle the fringes make with the vertical axis, and all other variables are defined as they are in Eqns. [1] through [5]. When the incident light is perfectly collimated, the period of the self image will be equal to that of the original grating. In this case, the fringes produced will be horizontal, as we saw in Eqn. [8] earlier. As the beam moves away from collimation, the fringes will acquire a greater tilt from the horizontal; furthermore, fringes produced by divergent

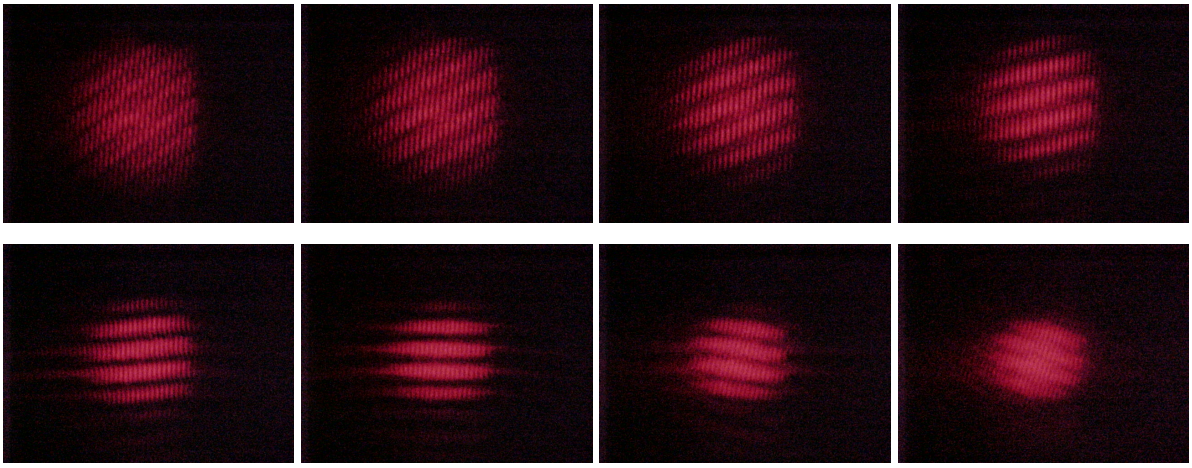

Figure 7: Moiré fringes recorded for different distances from the first lens (see Fig. 6). The images correspond to picture numbers 709, 714, 719, 724, 729, 734, and 744 shown in Table 1.

light will tilt in an opposite direction from fringes produced by convergent light. Thus, the tilt of the moiré fringes with respect to the horizontal would indicate unequivocally whether the beam is collimated, convergent, or divergent.

3.4 Results

We took pictures of moiré fringes for 40 different distances of the collimating lens from the first lens. The photographs were transferred to a computer using a floppy disk for further analysis. The fringe angles in the images were measured using *ImageJ* [34], a Java image processing and analysis software. This program was chosen because it had a tool that allowed the user to draw a line along the fringe direction to measure the angle relative to a reference line. Five angle measurements were taken for each picture and the results were averaged. The standard deviation of the five measurements was also calculated in order to get an idea of the variations within the set of five measurements. The data are given in Table 1. The results are summarized in Fig. 8, which shows a plot of fringe tilt from vertical versus distance from first lens. There seems to be a roughly linear relation between fringe tilt from the vertical and distance from the first lens. Work is under way to interpret Fig. 8 in a more quantitative manner.

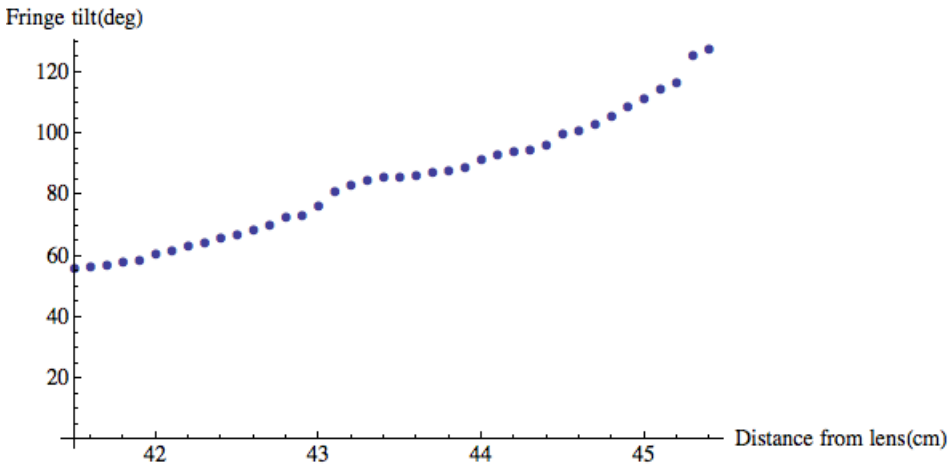

Figure 8: Fringe tilt from the vertical as a function of distance from the first lens.

4 Summary and Future Research

Creating moiré patterns by computer simulation is not the same as having a mathematical expression for them. In the future, we would like to better understand and extend previous work of this type, such as that of Creath and Wyant (1992) [18], Oster et al. (1964) [19], Amidror (2003) [22], and Gabrielyan (2002) [35]. We intend to relate the moiré patterns on elliptical gratings to the eccentricity of the overlapped ellipses. We further plan to observe and study the Glass patterns created by quasiperiodic gratings. We are especially interested in deriving the mathematics for moiré patterns created with quasiperiodic gratings, such as the sunflower floret patterns that were modeled. We are also interested in finding different kinds of quasiperiodic patterns to model.

The collimation tester experiment is still being conducted. A model will be created of the setup on *Mathematica* and compared with the results of the collimation test instrument. In addition, we will attempt to better understand what "collimation" means through this experiment. We hope to quantify the setup on *Mathematica* so that a user can input some information and receive as output information about how to move the collimating lens so that the beam is collimated.

Moiré patterns are more than a fascinating optical phenomenon; they also have a huge host of applications in the real world. They can aid in understanding topics that are at the forefront of science, such as graphene and quasicrystals, and provide simpler and faster methods of certain tasks

Table 1. Fringe tilt from vertical (degrees)

Picture number	Distance from lens *cm*	Meas. 1 *deg*	Meas. 2 *deg*	Meas. 3 *deg*	Meas. 4 *deg*	Meas. 5 *deg*	Avg. Tilt *deg*	S.D. *S*
709	41.5	56.00	56.48	55.85	56.53	55.84	56.14	.339
710	41.6	56.37	56.55	56.50	56.61	56.39	56.48	.103
711	41.7	56.88	57.41	56.37	57.36	57.09	57.02	.423
712	41.8	58.22	58.78	58.13	57.94	57.37	58.09	.509
713	41.9	59.00	59.41	58.57	58.70	59.09	58.95	.332
714	42.0	61.31	61.00	60.69	61.06	60.97	61.01	.222
715	42.1	62.07	62.33	62.45	61.84	62.16	62.17	.236
716	42.2	63.43	63.07	63.59	63.38	63.97	63.49	.329
717	42.3	64.38	64.34	64.32	64.65	64.48	64.43	.136
718	42.4	66.20	66.38	65.93	66.08	66.04	66.13	.172
719	42.5	66.72	66.90	67.55	66.14	67.98	67.06	.720
720	42.6	68.20	68.57	69.14	68.41	69.04	68.67	.405
721	42.7	70.04	70.22	70.28	70.21	70.18	70.19	.089
722	42.8	71.23	72.08	71.86	72.88	72.79	72.77	1.827
723	42.9	73.11	73.85	73.48	73.64	73.69	73.56	.281
724	43.0	75.74	76.42	76.55	76.59	76.40	76.34	.345
725	43.1	80.90	80.34	81.91	89.97	81.77	81.18	.654
726	43.2	83.35	82.96	83.48	83.04	83.02	83.17	.230
727	43.3	84.90	84.98	84.57	84.42	84.84	84.74	.237
728	43.4	86.08	86.15	86.30	86.08	86.58	86.24	.211
729	43.5	86.18	85.88	86.07	86.25	85.45	85.97	.321
730	43.6	86.80	86.71	86.47	86.19	86.78	86.59	.260
731	43.7	88.39	87.05	87.42	87.06	87.15	87.41	.566
732	43.8	87.94	88.21	87.56	88.12	88.17	88.00	.267
733	43.9	89.29	89.00	88.99	89.19	89.04	89.10	.132
734	44.0	91.65	91.53	91.64	91.33	91.59	91.55	.131
735	44.1	93.42	93.77	93.37	93.78	93.21	93.51	.254
736	44.2	94.37	94.21	94.42	94.33	94.49	94.36	.105
737	44.3	93.95	95.54	95.35	95.26	95.05	95.03	.629
738	44.4	96.05	96.84	96.97	97.09	96.28	96.64	.455
739	44.5	99.52	100.81	99.93	99.95	100.12	100.07	.471
740	44.6	100.56	101.16	101.47	101.48	101.67	101.27	.436
741	44.7	102.53	102.46	103.58	103.01	103.67	103.05	.567
742	44.8	105.86	105.13	105.84	106.06	106.22	105.82	.417
743	44.9	108.99	108.74	108.78	109.14	108.95	108.92	.163
744	45.0	111.14	111.60	111.67	112.13	111.96	111.76	.380
745	45.1	114.30	114.76	114.84	114.90	115.06	114.77	.286
746	45.2	116.92	116.57	117.49	116.87	117.10	116.99	.338
747	45.3	125.89	125.26	124.97	125.88	125.49	125.50	.398
748	45.4	128.04	128.28	128.14	128.09	127.59	128.03	.261

that are invaluable to optics research, such as collimation testing and focal length measurement. Understanding the moiré effect can help digital photographers to prevent aliasing in photographs and movies, and make more effective anti-counterfeit prevention measures. It is very likely that the moiré effect will find even more practical applications in the future. From a theoretical perspective, however, moiré patterns are, and will remain, a testament to the stunning beauty in mathematics that can be found if one knows where to look.

References

[1] Wesifall, R. (1962). *U.S. Patent No. 3,060,584*. Washington, DC: U.S. Patent and Trademark Office.

[2] Petrovsky, V. A. *et al.* (1980). *U.S. Patent No. 4,184,156*. Washington, DC: U.S. Patent and Trademark Office.

[3] Takeuchi, Y. (1988). *U.S. Patent No. 4,759,373*. Washington, DC: U.S. Patent and Trademark Office.

[4] mohair. (n.d.). *Collins English Dictionary - Complete Unabridged 10th Edition)*. Retrieved September 25, 2012, from Dictionary.com. website: *http://dictionary.reference.com/browse/mohair.*

[5] Harmuth, L. (1915). *Dictionary of textiles*. Fairchild publishing company. p. 106. Retrieved September 25, 2012.

[6] Brooks, R. E., & Heflinger, L. O., "Moiré Gauging Using Optical Interference Patterns," Applied Optics **8**, 939 (1969).

[7] Post, D., & Han, B., "Moire Interferometry," Springer Handbook of Experimental Solid Mechanics, (Ed.) W. N. Sharpe (2008).

[8] Kothiyal, M. P., & Sirohi, R. S., "Improved collimation testing using Talbot interferometry," Applied Optics **26**, 4056 (1987).

[9] Bhattacharya, J. C. and Aggarwal, A. K., "Measurement of the focal length of a collimating lens using the Talbot effect and the moir technique," Applied Optics **30**, 4479 (1991).

[10] Minnetonka, Paul S. Petersen (1971). *U.S. Patent No. 3,581,275*. Washington, SC: U.S. Patent and Trademark Office.

[11] Ragulskis M., & Aleksa A., "Image hiding based on time-averaging moiré," Opt. Commun. **14**, 2752 (2009).

[12] Counterfeit prevention Amidor, I. S., & Hersch, R. D., "Moiré methods for the protection of documents and products: a short survey," ICSXII Journal of Physics: Conference Series **77**, (2007).

[13] "The 2010 Nobel Prize in Physics - Press Release". Nobelprize.org. 27 Sep 2012 http://www.nobelprize.org/nobel_prizes/physics/laureates/2010/press.html.

[14] Macdonald, A. H., & Bistritzer, R., "Graphene moir mystery solved?," Nature, **464**, 453 (2011).

[15] See for e.g. Takasaki, H., "Moiré Topography," Applied Optics, **9**, 1467 (1970).

[16] Wolfram *Mathematica,* `http://www.wolfram.com/mathematica/`.

[17] Vogel, H., "A better way to construct the sunflower head," Math. Biosciences **44**, 179 (1979).

[18] Creath, K., & Wyant, J. C., "Moiré and fringe projection techniques, in Optical Shop Testing, D. Malacara, ed. (Wiley, 1992), pp. 653-660.

[19] Oster, G., et al., "Theoretical interpretation of moiré patterns," J. Opt. Soc. Am. **54**, 169 (1964).

[20] Merte, L. R., *et al.*, "Water-mediated proton hopping on an Iron Oxide surface," Science **633**, 889 (2012).

[21] Glass, L., & Pérez, R., "Perception of random dot interference patterns," Nature, **246**, 360 (1973).

[22] Amidror modification to Glass Amidror, I., "Glass patterns as moiré effects: new surprising results," Optics Letters, **28**, 7 (2003).

[23] "The Nobel Prize in Chemistry 2011 - Press Release". Nobelprize.org. 27 Sep 2012 http://www.nobelprize.org/nobel_prizes/chemistry/laureates/2011/press.html.

[24] Shechtman, D., & Blech, I., "The microstructure of rapidly solidified Al6Mn, Metallurgical Transactions, **16A**, 1005 (1985).

[25] Dinlap, R. A., "The Golden Ratio and Fibonacci Numbers," World Scientific (1998).

[26] Mudassar, A. A., & Butt, S., "Improved collimation testing technique," Applied Optics, **51**, 6429 (2012).

[27] Schaaf, L. J., "The Photographic Art of William Henry Fox Talbot." Princeton: Princeton University Press, (2000).

[28] Lord Rayleigh, "On copying diffraction-gratings, and on some phenomena connected therewith, Phil. Mag., **11**, 196 (1881).

[29] Cowley, J. M., & Moodie, A. F., "Fourier Images: I The point source, Proc. Phys. Soc., **70**, 486 (1957).

[30] Winthrop, J. T., & Worthington, "Theory of Fresnel images. I. Plane periodic objects in monochromatic light, J. Opt. Soc. Am., **55** (1965).

[31] Berry, M. V., & Klein, S., "Integer, fractional and fractal Talbot effects, J. Mod. Opt., **43**, 2139 (1996).

[32] Ganesan 1993 Ganesan, A. R., & Venkateswarlu, P., "Laser beam collimation using Talbot interferometry," Applied Optics, **32**, 2918 (1993).

[33] Silva, D., "A simple interferometric method of beam collimation," Applied Optics, **10**, 1980 (1971).

[34] ImageJ, http://rsbweb.nih.gov/ij/.

[35] Gabrielyan, E., "The basics of line moir and optical speedup, arXiv:physics/0703098 (2007).